Bioorganic Chemistry 112 (2021) 104951

Contents lists available at ScienceDirect

Bioorganic Chemistry

journal homepage: www.elsevier.com/locate/bioorg

Diversity-oriented synthesis through gamma radiolysis: Preparation of unusual ecdysteroid derivatives activating Akt and AMPK in skeletal muscle cells

Halima Meriem Issaadi [a,1,2], Zoltán Béni [b,1], Tünde Tóth [c,d], Miklós Dékány [b], Tusty-Jiuan Hsieh [e], György Tibor Balogh [f,g,*], Attila Hunyadi [a,h,*]

[a] Institute of Pharmacognosy, University of Szeged, Eötvös str. 6, 6726 Szeged, Hungary
[b] Spectroscopic Research, Gedeon Richter Plc., Gyömröi út 19-21, H-1103 Budapest, Hungary
[c] Department of Organic Chemistry and Technology, Budapest University of Technology and Economics, PO Box 91, H-1521 Budapest, Hungary
[d] Institute for Energy Security and Environmental Safety, Centre for Energy Research, P.O. Box 49, H-1525 Budapest, Hungary
[e] Graduate Institute of Medicine, Kaohsiung Medical University, Kaohsiung 807, Taiwan, ROC
[f] Department of Chemical and Environmental Process Engineering, Budapest University of Technology and Economics, Budafoki út 8., H-1111 Budapest, Hungary
[g] Faculty of Pharmacy, Department of Pharmacodynamics and Biopharmacy, University of Szeged, Eötvös utca 6., H-6720 Szeged, Hungary
[h] Interdisciplinary Centre for Natural Products, University of Szeged, Eötvös str. 6, 6720 Szeged, Hungary

ARTICLE INFO

Keywords:
Gamma radiolysis
Ecdysterone
Natural product
Diversity-oriented synthesis
Centrifugal partition chromatography
Protein kinase B
AMP-activated protein kinase

ABSTRACT

Gamma-ray radiation is a unique way to induce chemical transformations of bioactive compounds. In the present study, we pursued this approach to the diversity-oriented synthesis of analogs of 20-hydroxyecdysone (20E), an abundant ecdysteroid with a range of beneficial, non-hormonal bioactivities in mammals including humans. Gamma irradiations of aqueous solutions of 20E were conducted either in N_2- or N_2O-saturated solutions. Centrifugal partition chromatography was used to fractionate crude resulting irradiated materials using a biphasic solvent system composed of *tert*-butyl alcohol - ethyl acetate - water (0.45:0.9:1, v/v/v) in ascending mode. Subsequently, the products were purified by RP-HPLC. Fourteen ecdysteroids, including five new compounds, were isolated, and their structure were elucidated by 1D and 2D NMR and HRMS. Compounds **2**–**4**, **7**, **9**, **12** and **15** were tested for their capacity to increase the Akt- and AMPK-phosphorylation of C2C12 murine skeletal myotubes *in vitro*. The compounds were similarly active on Akt as their parent compound. Stachysterone B (**7**) and a new ring-rearranged compound (**12**) were more potent than 20E in activating AMPK, indicating a stronger cytoprotective effect. Our results demonstrate the use of gamma irradiation in expanding the chemical diversity of ecdysteroids to obtain new, unusual bioactive metabolites.

1. Introduction

Phytoecdysteroids, herbal analogs of the insect molting hormone, are well-known for their versatile chemistry and the wide range of non-hormonal, beneficial bioactivities in mammals including humans [1]. Among these bioactivities, the anabolic and adaptogenic activity of the most abundant ecdysteroid, 20-hydroxyecdysone (20E), is probably the best known [2]. Thanks to these, a plethora of ecdysteroid-containing food supplements are available worldwide [3], and their consumption raised concerns on their possible abuse in sport performance enhancement [4,5]. Because of this, 20E is currently on the watchlist of the World Anti-Doping Agency (WADA), with a possibility to become a doping-controlled substance soon [6]. As a possible therapeutic agent, 20E is also the subject of ongoing clinical trials in patients with sarcopenia [7] or pre-diabetic conditions [8].

The structural diversity of ecdysteroids can be translated into a versatile and diverse pharmacology that is largely unexplored in mammals. Some pairs of derivatives may exert completely opposite

* Corresponding authors.
E-mail addresses: balogh.gyorgy@vbk.bme.hu (G.T. Balogh), hunyadi.attila@szte.hu (A. Hunyadi).
[1] Equal contribution by the first two authors.
[2] Present address: Laboratory of Chromatography, Faculty of Chemistry, University of Sciences and Technology Houari Boumediene, BP 32 Bab Ezzouar, 16111, Algiers, Algeria.

https://doi.org/10.1016/j.bioorg.2021.104951
Received 27 January 2021; Received in revised form 22 April 2021; Accepted 26 April 2021
Available online 29 April 2021

bioactivities, for example, we have previously demonstrated that 20E protects ABCB1-transfected multi-drug resistant lymphoma cells from the cytotoxicity of doxorubicin, while its diacetonide derivative strongly decreased the same cell line's doxorubicin resistance [9]. Ecdysteroids' effect on cell death and survival appears to follow a similar pattern for side-chain shortened compounds and their apolar analogs substituted with a ketal function on their A-ring [10–12]. Further, calonysterone and its desmotrope pair, isocalonysterone showed opposite effects on the phosphorylation of protein kinase B (Akt) [13] that is among the effectors of ecdysteroids' action on cell death and survival, and on protein synthesis [11,14].

Chemical consequences of the interaction between high-energy ionizing radiation, such as gamma rays, and matter, are of interest for a wide range of disciplines from astrobiology to radiation chemistry [15–17]. The impact of gamma irradiation on certain types of steroids was previously studied in solid phase, considering that such radiation may be applied for the sterilization of pharmaceuticals. Upon gamma irradiation, cholesterol was reported to suffer oxidation on its rings A and B [18]. Gamma irradiation-induced changes in the structure of corticosteroids were observed in two major directions, i.e. side-chain cleavage forming C17 ketones, and oxidation of the C-11 alcohol to the C-11 ketone [19]. Ergosterol and calciferol were also found to be sensitive to irradiation-induced oxidation in the presence of oxygen, and the irradiation of calciferol afforded a peroxide and other non-peroxidic substances [20]. To the best of our knowledge, the effect of gamma irradiation on the chemical structure of ecdysteroids has not been studied before.

During the gamma radiolysis of water, high-energy electrons are generated that initiate a large variety of reactions that lead to the formation of primary reactive intermediates, i.e. hydroxyl radicals ($HO^{\bullet}$), hydrated aqueous electrons (e^{-}) and hydrogen radicals ($H^{\bullet}$) that can react with organic compounds through various mechanisms [21]. Recently, we have been pursuing the drug discovery potential of diversity-oriented synthesis using biorelevant reactive oxygen species (ROS) on antioxidants that may scavenge them [22–24]. While they are not classical, phenolic antioxidants, ecdysteroids have been reported to efficiently counteract oxidative stress *in vitro* [25] and *in vivo* [26].

Based on the above considerations, in the current study it was our aim to elaborate the potential of gamma ray irradiation in aqueous medium to serve as a preparative tool to further expand the chemical diversity of ecdysteroids towards new, possibly bioactive metabolites. Further, as a first bioactivity testing to assess the potential anabolic and cytoprotective activity of the newly prepared compounds, we aimed to evaluate their activity on the protein kinase B (Akt) and AMP activated kinase (AMPK) phosphorylation of skeletal muscle cells.

2. Materials and methods

2.1. Materials

The starting material, 20-hydroxyecdysone, with a purity of 90%, originated from the roots of *Cyanotis arachnoidea* was purchased from Shaanxi KingSci Biotechnology Co., Ltd. (Shanghai, China). The compound was recrystallized from ethyl acetate - methanol (2:1, v/v), so that purity of 20E utilized for the irradiations was 97.8%, by means of HPLC-DAD, maximum absorbance within the range of 220–400 nm.

Solvents used for the fractionation (*tert*-butyl alcohol and ethyl acetate) were of analytical grade, obtained from commercially available sources and were used without further purification. Acetonitrile used for the purification and purity analysis was of chromatographic grade, it was obtained from commercially available sources.

2.2. General methods

Preliminary analytical screening of the irradiated materials was performed by using HPLC-ESI-MS system on a Waters Cortecs C18 (2.7 μm, 150 × 4.6 mm) column and ESI source in positive mode.

Compounds were fractionated by using Centrifugal Partition Chromatography on an Armen Spot CPC 250 mL (Armen Instrument, Saint Ave, France) system composed of an Armen Spot Prep II equipment and an Armen Spot CPC multilayer coil separation column and controlled by the Armen Glider CPC software. Optimization of the CPC separation was through following well-established general strategies [27–29].

Semi-preparative purifications over RP-HPLC were carried out on an Agilent 1100 series (Waters Co., Milford, MA, USA) connected to a Jasco UV-2075 detector (Jasco Co., Tokyo, Japan) utilizing a Luna Phenyl-Hexyl (5 μm, 250 × 10 mm) column.

Preparative purifications over RP-HPLC were performed on CPC instrument by switching from the CPC multilayer coil separation column to either a Kinetex XB C18 (5 μm, 250 × 21.2 mm) column or a Kinetex Biphenyl (5 μm, 250 × 21.2 mm) column.

Purity of the obtained compounds was determined by RP-HPLC analyses on a system of two Jasco PU-2080 pumps, a Jasco AS-2055Plus intelligent sampler connected to a JASCO LC-Net II/ADC equipped with a Jasco MD-2010 Plus PDA detector (Jasco Co., Tokyo, Japan) utilizing a Kinetex Biphenyl (5 μm, 250 × 4.6 mm) column, applying an isocratic 20% aq. Acetonitrile mobile phase at a flow rate of 1 mL/min.

2.3. Mass spectrometry

HRMS and MS-MS analyses were performed on a Thermo LTQ FT Ultra or a Thermo Velos Pro Orbitrap Elite (Thermo Fisher Scientific) system using ESI ionization method operating in positive ion mode. The protonated molecular ion peaks were fragmented by CID using helium as collision gas at a normalized collision energy of 35 to 55%. The samples were dissolved in methanol before analysis. Data acquisition and analysis were accomplished with Xcalibur software version 4.0 (Thermo Fisher Scientific).

2.4. NMR spectroscopy

NMR spectra were recorded on a Bruker Avance III HD 500 MHz or a Varian VNMRS 800 MHz NMR spectrometer, equipped with a liquid helium cooled 5 mm TCI CryoProbe or with a 5 mm HCN ^{13}C enhanced salt tolerant cold probe, respectively. Data were collected in CD_3OD as solvent at 298 K in all cases, except for **5**, where spectra were also acquired in a 1 to 1 mixture of CD_3CN/D_2O at 318 K. Chemical shifts are referenced to residual solvent signal signals (3.31 ppm for ^{1}H and 49.15 for ^{13}C in CD_3OD or 2.06 ppm for ^{1}H and 121.9 ppm for ^{13}C in CD_3CN/D_2O). Standard one (^{1}H and ^{13}C) and two dimensional (COSY/TOCSY, HSQC, HMBC and ROESY) data were recoreded in all cases using the pulse sequences available in the Bruker Topspin 3.5 p7 or in the VNMRJ 3.2 sequence libraries. In case of **5** ^{1}H, COSY and ROESY data were acquired using presat solvent supression. ACD/Spectrus Processor 2017.1.3 software (ACD/Labs, Canada) was used for data interpretation and reporting.

2.5. Molecular modelling

A molecular modelling study was performed with Macromodel (Schrödinger Release 2019–4: MacroModel, Schrödinger, LLC, New York, NY, 2019) and Jaguar (Schrödinger Release 2019–4: Jaguar MacroModel, Jaguar, version 10.4, Schrodinger, Inc., New York, NY, 2019 [30]) software packages. Firstly, an MM level conformational search was performed using mixed torsional low mode sampling with the OPLS3 force field. A 5.02 kcal/mol energy window was applied for saving structures setting $CHCl_3$ as solvent. After this, the geometry optimization of the representative conformers (two conformers in the case of **5** and one in the case of **6**) were undertaken at the DFT level using standard B3LYP-D3 functional and 6-31G**+ basis sets. Then NMR shielding values were calculated in a single point energy calculation on the optimized geometries using B3LYP-D3 functional, 6-311G**+ basis

set and PBF solvent model of methanol. Finally, DP4 statistical analysis of the resulted shieldings of the two conformers of **5** with respect to the experimental chemical shifts was carried out using the template published by Grimblat, Zanardi and Sarotti [31].

2.6. Gamma-irradiations

2.6.1. Small scale gamma-irradiations

Solutions containing 200 mg of 20E in 833 mL of water (0.5 mM) were prepared and saturated by N_2 or N_2O. The solutions were irradiated at room temperature using a ^{60}Co source, panoramic type γ-irradiation facility (dose rate = 10 kGy/h). The absorbed dose, i.e. the energy absorbed in unit mass of the aqueous solution (J/kg = Gy), was 1 or 2 kGy. Dose rate was determined by using the ethanol-chlorobenzene dosimetry system according to ISO/ASTM 51538, 2009 standard, traceable to the accredited Dosimetry Laboratory, Danish Technical University, Denmark. Dosimetry was performed in the same glass vessel and irradiation position as the samples' setup. The final irradiated materials were lyophilized as follows. The aqueous solution was divided into 4 × 250 mL stocks and transferred to four 1 L round-bottom flasks. Then, the aqueous solution was frozen crustally on the wall of round-bottomed flasks in acetone/dry ice bath using a Büchi RE 121 Rotavapor at 60 rpm under atmospheric pressure. Lyophilization was then performed using a Christ Alpha 2-4LD Plus instrument (operational parameters: −85 °C under 0.1 mbar for 24–48 h). The lyophilizate residues were combined and analysed with HPLC-ESI-MS. The aqueous solutions of 20E irradiated in N_2– or N_2O-saturated solution that absorbed a dose of 2 kGy were selected for purification. Due to the low amounts of the residues, the samples were dissolved in methanol (HPLC grade) and directly subjected to preparative RP-HPLC using a Kinetex XB C18 (5 µm, 250 × 21.2 mm) column with 20% aqueous acetonitrile at a flow rate of 16 mL/min. The obtained fractions were evaporated using a rotary evaporator at 40 °C. Compounds **3** and **4** were obtained from both irradiations, whereas compound **2** resulted only from the irradiation in N_2-saturated solution. Compounds **5** and **6** coincided in one single fraction only from the irradiation in N_2O-saturated solution.

2.6.2. Large scale gamma-irradiations

Irradiation procedure. Two solutions (**I** and **II**), each containing 1 g of 20E in 1041 mL of water (2 mM), were prepared. Irradiations were performed similarly as above (dose rate = 10 kGy/h, absorbed dose = 6 kGy), either in N_2-saturated (solution **I**) or in N_2O-saturated solution (solution **II**). Each final irradiated material was lyophilized as described above, and 838 mg of residue **I** and 843 mg of residue **II** were obtained.

Fractionation of the product mixtures by centrifugal partition chromatography. Residues **I** and **II** were fractionated by CPC with a biphasic solvent system composed of *tert*-butyl alcohol - ethyl acetate - water (0.45:0.9:1, v/v/v) in ascending mode, and an altogether 95.71% and 97.35% of the initial weights of residue **I** and **II**, respectively, were recovered after the separation. The selection of the biphasic solvent system was achieved by the evaluation of the partition coefficients K. Briefly, the K-values were determined by HPLC analysis as follows: the same volume of the upper and the lower phases of each biphasic tested solvent system were introduced in test tubes and approximately 0.5 mg of crude irradiated material was added. The tubes were sonicated and shaken with a vortex mixer (VWR, Lab dancer S40). Subsequently, an equal volume of each phase was analysed by HPLC. The K-values were expressed as the peak area of each targeted compound in the upper phase divided by that in the lower phase. In order to find the most suitable CPC biphasic system, nine solvent systems were studied and three of them gave satisfactory partitioning of the targeted compounds between the two phases, with K values falling within the range of 0.5–16 [32] (Table S16). The selected biphasic solvent system gave optimal values concerning the settling time (24 s), the volume ratio of the upper and lower phases (0.95) and the retention volume ratio Sf (0.52).

After selecting the optimal solvent system, a total volume of 2400 mL of this mixture was prepared in a 5 L separation funnel, vigorously shaken, and thoroughly left to equilibrate. the upper organic phase was selected as the mobile phase and the lower aqueous phase was used as the stationary phase in ascending mode (tail-to-head way). The sample solution was prepared by dissolving each irradiated material in the mixture solution of lower phase and upper phase (1:1, v/v) of the solvent system. The CPC separation was performed, with optimized parameters, as follows: the multilayer coiled column was first filled in descending mode with the stationary phase with a high flow rate of 50 mL/min at a rotation speed of 500 rpm and pressure of 17 bar. Then the mobile phase was introduced in ascending mode into the column with a flow rate of 10 mL/min at a pressure of 87 bar and a rotation speed of 1600 rpm gradually adjusted to 2900 rpm to generate a centrifugal acceleration. After the hydrodynamic equilibrium was reached, the sample solution was injected into the column through the inject valve. The effluent of the column was continuously monitored with a UV detector at 243 nm and 300 nm and collected.

RP-HPLC purifications. The combined CPC fractions were evaporated using a rotary evaporator at 40 °C, dissolved in methanol (HPLC grade) and analysed by RP-HPLC. For the purification of combined CPC fractions of residues **I** and **II**, preparative (16 mL/min) or semi-preparative (3 mL/min) RP-HPLC techniques using different chromatographic columns were utilized as summarized in Table S19.

2.7. Bioactivity testing

Mouse C2C12 skeletal myoblasts (BCRC#60083) were purchased from the Bioresource Collection and Research Center (BCRC, Food Industry Research and Development Institute, Taiwan). The cells were seeded in 6 cm dishes and maintained in high-glucose Dulbecco's modified Eagle's medium (DMEM) with 10% (v/v) fetal bovine serum (FBS) and 1% penicillin/streptomycin solution in a humidified atmosphere of 95% air and 5% CO2 at 37 °C. To induce differentiation, 100% confluent C2C12 myoblasts were cultured in DMEM containing 450 mg/dL D-glucose and 10% horse serum. The medium was changed every other day. When the cells became skeletal myotubes, the culture medium was changed to FBS free normal-glucose (100 mg/dL) DMEM with or without 10 µM of each test compound for 2 h to test the activity on Akt and AMPK. Then, the cells were lysed with 700 µL of 1 × sample buffer (62.5 mM Tris-HCl, pH 6.8; 10% glycerol; 2% SDS, sodium dodecyl sulfate; 50 mM DTT, dithiothreitol; 0.0025% bromophenol blue), sonicated for 15 s, and heated to 95 °C for 5 min. For analysis of proteins, the cell lysate was loaded and separated on 10% SDS-polyacrylamide gels. Proteins were then transferred to PVDF membranes and detected using phosphorylated and total Akt or AMPK antibodies (Cell Signaling Technology, Inc., Danvers, MA, USA).

3. Results and discussion

3.1. Preliminary investigations

Gamma irradiations of 20-hydroxyecdysone were performed targeting structural modifications of the whole starting material with an interesting chemistry never explored for ecdysteroids before. As a first step, small scale irradiations in N_2- or N_2O-saturated aqueous solutions of 20E were performed at 10 kGy/h dose rates with absorbed doses of 1 or 2 kGy. N_2 or N_2O saturation was selected to distinguish between oxidative (former) or reductive (latter) processes during the irradiations, and the applied dose was selected based on our previous experience in similar studies on other compounds [33]. The preliminary HPLC-ESI-MS analysis of the resulted materials showed that the same product patterns were obtained at both absorbed doses. However, the applied gas had an influence on the peak ratio of the observed resulting products (see Supplementary Fig. S1). Consequently, the irradiations performed in N_2- or N_2O-saturated solutions with an absorbed dose of 2 kGy were selected for purification over preparative RP-HPLC.

Purification of the irradiated material in N_2-saturated solution resulted in the isolation of 14-hydroperoxy-20E (**2**, 4.82 mg, 2.59%), **3** (0.96 mg, 0.54%) and podecdysone B (**4**, 0.53 mg, 0.31%) whereas purification of the one irradiated under N_2O-saturated solution allowed the isolation of compound **3** (3.53 mg, 2.35%), podecdysone B (**4**, 1.70 mg, 1.16%) and 2-dehydro-20E (**5**) and 2-dehydro-3-*epi*-20E (**6**) coincided in one single fraction (5:1 ratio, compound **5** being the major component) (1.10 mg).

3.2. Large scale gamma irradiations of 20E

To obtain larger amounts of the above products and to isolate further minor compounds, the irradiations were scaled-up. Larger scale irradiations were performed at dose rate of 10 kGy/h with absorbed doses of 6 kGy in N_2- or N_2O-saturated solutions. The resulting irradiated materials were lyophilized, and the obtained dry residues were fractionated by CPC with a biphasic solvent system composed of *tert*-butyl alcohol - ethyl acetate - water (0.45:0.9:1, v/v/v) in ascending mode. Combined CPC fractions were purified from minor impurities by RP-HPLC. From the irradiation of N_2-saturated aqueous solution of 20E, the same compounds were obtained as for the small-scale irradiation, i.e., 14-perhydroxy-20E (**2**), compound **3** and podecdysone B (**4**). These were accompanied by stachysterone B (**7**), 14-deoxy-20E (**8**), 5α-20E (**9**), a 7-11′ heterodimer (**11**), and compound **12**. Concerning the irradiation in N_2O-saturated solution, compound **3**, podecdysone B (**4**), 2-dehydro-20E (**5**), stachysterone B (**7**), 5α-20E (**9**), 2-dehydro-3-deoxy-20E (**10**), compound **12**, compound **13**, 25-hydroxy-dacryhainansterone (**14**) and 22-dehydroecdysone (**15**) were isolated. A detailed description of the structure elucidation of these compounds is presented in Section 3.3, percent yields of all isolated products from large-scale irradiations under N_2- and N_2O-saturated aqueous solution of 20E are listed in Table 1, and their chemical structures are presented in Fig. 1.

The products were isolated in low to very low yields, which is partially explained by their chromatographic overlapping. Because of the complex minor product patterns (see Supplementary Information, Figs. S2-S3), we did not aim for a complete isolation of any of the products, instead, their isolation was terminated when amounts enough for structure elucidation were obtained.

Close observation of the irradiated products showed that major modifications took place in the B, C and/or D rings of the starting material. For example, only compounds **5**, **6** and **10** presented modifications in the ring A where the 2β-hydroxyl group was oxidized to a keto-group.

It may be of interest that some compounds related to those obtained in our study were previously reported from the UV-induced photochemical transformations of 20E. For example, Canonica et al. reported the hydroperoxyde compound **2** and the 14-epimer of compound **8** from the irradiation of 20E by a Pyrex-filtered high-pressure Hg lamp [34], and Harmatha et al. reported a 7,7′-homodimer of the $\Delta^{8,14}$ olefin-containing unit of compound **11** as the main product from a similar irradiation by a medium-pressure lamp [35]. This relationship between the possible products of 20E from photolysis and gamma radiolysis is because free radicals are involved in both. Nevertheless, the overall reaction mechanisms and therefore the expectable product patterns are significantly different: while the photolysis of enones is initiated by the formation of a biradical and the products are determined by subsequent rearrangements [34], gamma radiolysis in aqueous solution is rather driven by reactive species formed from the solvent [21].

Table 1
Percent yields of the isolated products from large-scale irradiations of 20E.

N_2-saturated		N_2O-saturated	
CPC Fractions	Products	CPC Fractions	Products
1–12	**4** (4.06 mg, 0.50%)	1–16	**4** (6.76 mg, 0.83%) **10** (0.90 mg, 0.11%)
13–14	**7** (6.61 mg, 0.82%) **8** (2.00 mg, 0.25%)	17–20	**7** (1.20 mg, 0.15%) **9** (1.00 mg, 0.37%)
15–16	**2**(13.15 mg, 1.52%)	21–27	**5** (0.70 mg, 0.08%)
17–18	**9** (2.62 mg, 0.31%)	28–31	**13** (1.50 mg, 0.18%)
21–26	**1** (257.96 mg)	32–36	**1** (387.66 mg)
27–30	**3** (7.79 mg, 0.94%)	37–45	**3** (18.18 mg, 2.18%) **14** (1.00 mg, 0.12%)
31–39	**11** (1.20 mg, 0.07%)	48–54	**12** (2.27 mg, 0.27%)
40–43	**12** (1.48 mg, 0.18%)	63–73	**15** (2.66 mg, 0.33%)

3.3. Structure elucidation

Compounds **2** [36], **4** [37 38], **7** [39], **8** [40], **9** [41], **10** [42], **14** [43] and **15** [44] were reported earlier in the literature. Our HRMS and NMR data (see Supplementary Information, Figs. S4, S5, S11-12, S23-30 and S46-49, and Tables S1-8) were in good agreement with the published data.

For compound **3**, HRMS data indicated an elemental composition of $C_{27}H_{42}O_7$ (Fig. S10). Thus, nominally, the incorporation of a double bond to 20E (**1**) was assumed. In accordance with this, besides the doublet characteristic to H-7, another doublet of doublet was detected at 5.81 ppm in the ^{1}H NMR spectrum. In parallel, along with the resonances due to the 6-keto-Δ7 moiety (206.1, 122.5, 165.8 ppm), an alkenyl (125.0 ppm) and a quaternary (157.0 ppm) carbon resonance was detected in the aromatic region of the ^{13}C NMR spectrum (Fig. S6). Based on the HMBC correlations of H-18 (1.04 ppm) with C-12 (28.1), C-13 (52.9), C-14 (86.4), C-17 (157.0) together with those of H-21 (1.31 ppm) with C-17 (157.0), C-20 (77.7), C-22 (77.1) and the alkenyl proton at 5.81 ppm (H-16) with C-13 (52.9), C-14 (86.4), C-15 (39.1) and C-20 (77.7), the double bond formation between C-16 and C-17 was concluded. Further analysis of the HSQC, ROESY and HMBC data (Figs. S6-8) confirmed this suggestion and enabled the complete ^{1}H and ^{13}C NMR assignment of **3**. Based on the highly similar spectral features observed for **3** (except those belonging to ring D protons and carbons) and reported for **1** [45], the structure depicted in Fig. 1 was proposed for compound 3 that is a new ecdysteroid; complete NMR signal assignment of **3** is listed in Table 2.

Compounds **5** and **6** were obtained as a mixture (ca. 5 to 1 molar ratio based on the relative integrals of H-3 resonances). In line with their similar chromatographic behaviour, HRMS data suggested that **5** and **6** had an identical molecular formula of $C_{27}H_{42}O_7$ (Fig. S22). The ^{1}H and ^{13}C NMR spectral data showed that the two compounds are structurally highly similar both to each other and to **1** (Fig. S13). The most significant differences were observed for the signals belonging to the A and B rings' protons and carbons. First, as compared to **1**, the ^{1}H NMR spectrum (CD_3OD solution) presented only one A-ring OCH signal in both compounds **5** (dd 4.04 ppm) and **6** (dd at 4.34 ppm). Second, besides the significantly broadened signal assignable to the C-6 carbons of **5** (~201 ppm) and **6** (203.3 ppm), two further carbonyl signals were detected in the ^{13}C NMR spectrum at 212.1 (**5**) and 210.9 ppm (**6**). These findings indicated the oxidation of either the 2-OH or the 3-OH group in both compounds. The three TOCSY correlations of the OCH protons of both **5** (4.02/2.85, 1.76, 2.74) and **6** (4.34/2.18, 1.81, 2.66) suggested that **5** and **6** were the 2-dehydro analogs of **1**. Based on the good match between our ^{1}H and ^{13}C NMR data and those reported by Savchenko et al. in the same solvent [46] and to those reported by Sarker et al. in a different solvent [47] the minor component, **6** was unambiguously assigned as the 2-dehydro-3α-OH derivative of **1** (Fig. 1).

The analysis of the TOCSY, HSQC and HMBC (Figs. S13-14) data with the ^{1}H and ^{13}C assignments of **6** at hand, strengthened further the identical constitution of **5** and **6** and showed that the structural differences between these compounds concerned ring A only. Assuming that the configuration of C-10 was intact during the oxidation of **1**, with the structure of **6** at hand, three structural alternatives could be considered for **5** at this point. It could either be described as the C-3 or C-5 epimer of **6** or its 3β,5α diastereoisomer. With the inversion of C-5, thus with the change from *cis* to *trans* A/B ring junction, however, a significant ^{13}C

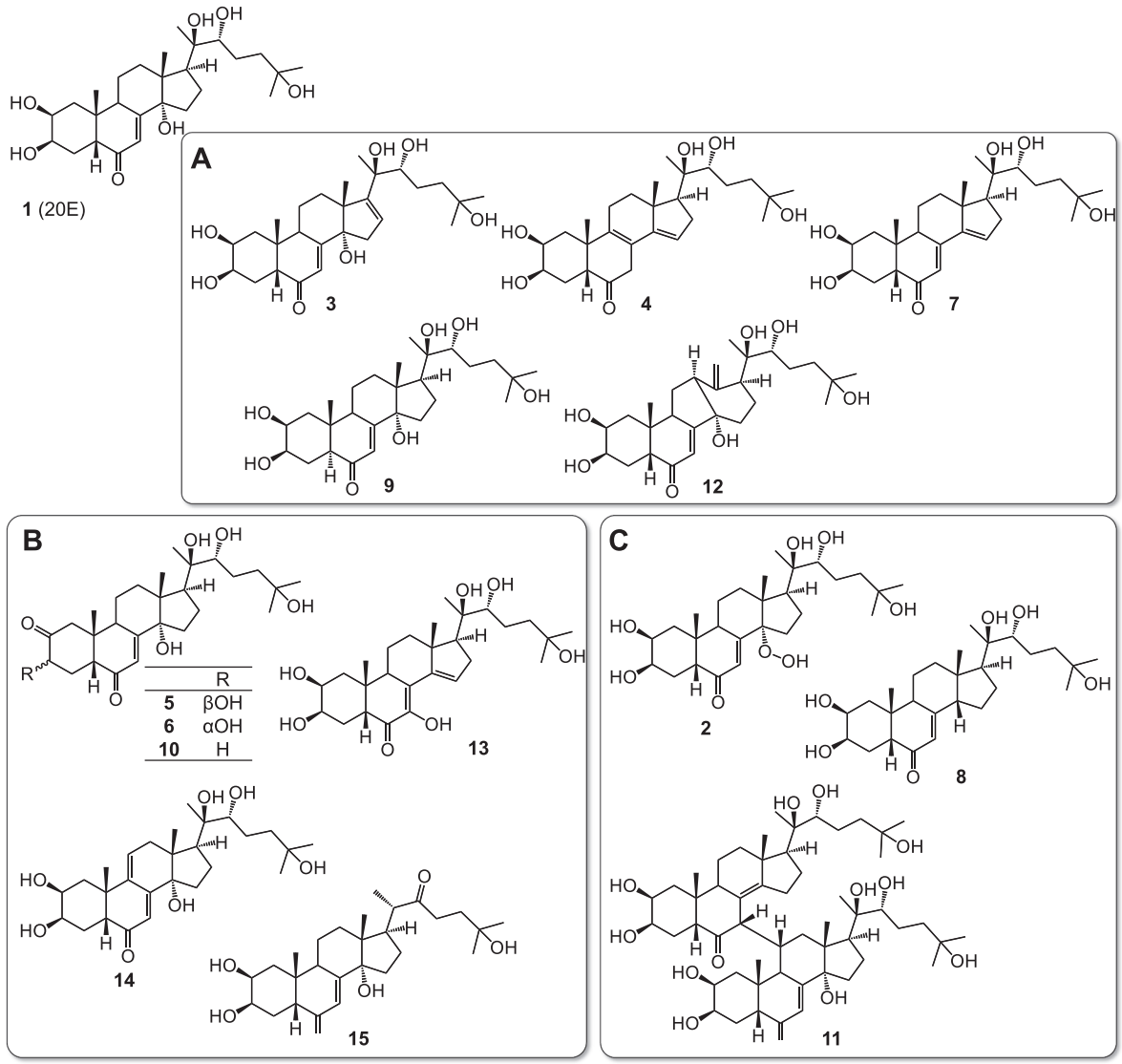

Fig. 1. Structures of 20-hydroxyecdysone (**1**, 20E), and its derivatives (**2**–**15**) obtained by gamma irradiations in aqueous medium. **A**: compounds obtained from both experimental setups (**3**, **4**, **7**, **9** and **12**), **B**: compounds obtained only from irradiation in N_2-saturated solution (**5**, **6**, **10**, **13**, **14** and **15**), and **C**: compounds obtained only from the irradiation in N_2O-saturated solution (**2**, **8** and **11**).

upfield shift of C-19 would have been expected, e.g. in the case of **9** δ(C-19) is 15.9 ppm whereas that of **1** is 24.4 ppm. Following this argument, the observed 24.6 ppm C-19 chemical shift in the case of **5** suggested a *cis* A/B junction, which then narrows down the structural possibilities to the 2-dehydro-3β-20-hydroxyecdysone structure for **5**. Regarding the stereochemistry, however, some ambiguity was found. First, with regard to the discussion on the conformational equilibrium of **6** reported by Girault et al. [48], and taking into account the axial position of H-3 (suggested by the 10.7 and 6.9 Hz coupling constants determined from its signal analysis), a twisted boat-like A-ring geometry (**5b**, Fig. 2A and S48) was envisaged for **5**. The largest, ca. 4 Hz coupling constant value estimated from the signal analysis of the broad H-5 resonance was, however, contradicting its axial position in this conformation. In parallel, while the observed NOE correlations of H-19/H-5, H-19/H-9, H-19/H-11β were in accordance with this geometry, the missing H-3/H-9 and the observed H-19/H-11α correlations contradicted it. Indeed, all these results pointed toward an unusual conformation, where ring-A adopted a chair-like geometry and H-5 occupied an equatorial position with respect to ring-A. Unfortunately, the significant line broadening of H-1, H-4, C-1, C-4 and C-9 in CD_3OD did not allow the unambiguous verification of this proposition.

Thus, a molecular modelling study was initiated, and the NMR measurements were repeated in a 1 to 1 mixture of CD_3CN/D_2O at 45 °C. Although, decomposition of **5** to its 5α epimer (inversion of C-5 and deuteration of H-5 most probably due to a keto-enol tautomerization of the 6-keto group in this solvent mixture; Figs. S14-19) was observed and some line broadening (especially H-4α) was still present, the complete ^1H and ^{13}C NMR assignment of **5** (Table 2) could be achieved in this solvent mixture at 45 °C temperature.

According to the MM level conformational search (using Macromodel) followed by the geometry optimization of the representative conformers at the DFT level [30] on a model system (the side chain was truncated to a Me group), **5** was shown to have two major conformers (energy components and xyz coordinates are listed in Tables S9-12). The energetically more favored one (ca. 18.8 kJ/mol and ca. 6.7 kJ/mol in the gas phase and in solution phase, respectively), **5a** exhibited a chair-like A-ring where H-3 occupied an axial and H-5 an equatorial position (Fig. 2A, left). While, **5b** (Fig. 2A, right) bore with a twisted boat-like A-ring, where both H-3 and H-5 occupied an axial position. Indeed, **5b** was the initially expected while **5a** was the envisaged conformation discussed above.

Further to the geometry optimization, NMR chemical shifts were

Table 2
NMR assignments of compound **3** in CD_3OD, and **5** in CD_3OD and CD_3CN/D_2O (1:1) solvent mixture.

	3			**5** in CD_3OD			**5** in CD_3CN/D_2O		
Atom#	$\delta^{13}C$, ppm	$\delta^{1}H$, ppm	mult (J in Hz)	$\delta^{13}C$, ppm	$\delta^{1}H$, ppm	mult (J in Hz)	$\delta^{13}C$, ppm	$\delta^{1}H$, ppm	mult (J in Hz)
1β	37.1	1.43	m	nd	nd		51.6	2.12	m
1α	37.1	1.79	m	nd	nd		51.6	2.76	m
2	68.4	3.83	dt (11.8, 3.8)	212.1	–		215.9	–	
3	68.3	3.95	m	73.6	4.02	dd (10.2, 6.7)	75.2	4.11	dd (11.0, 7.6)
4β	32.6	1.70	m	nd	1.76	m	33.1	1.85	m
4α	33.6	1.78	m	nd	2.85	m	33.1	2.84	br m
5	51.8	2.41		48.6	2.74	br m	49.9	2.80	m
6	206.0			201.3			204.6	–	
7	122.5	5.88	d (2.5)	120.9	5.86	d (1.2)	122.7	5.96	s
8	165.8			168.1			170.3	–	
9	34.6	3.22	m	49.7	2.79	dd (12.5, 5.4)	46.0	2.77	m
10	39.4			42.8			44.5	–	
11β	21.5	1.75	m	nd	1.72	m	27.7	1.72	m
11α	21.5	1.89	m	nd	1.88	m	27.7	1.93	m
12β	28.1	1.84	m	34.2	1.83	m	35.6	1.86	m
12α	28.1	2.44	m	34.2	2.05	m	35.6	1.97	m
13	52.9			52.6	–		54.6	–	
14	86.4			86.5	–		88.9	–	
15β	39.1	2.77	dd (15.9, 1.4)	30.6	2.06	m	32.1	2.11	m
15α	39.1	2.23	dd (15.9, 3.4)	30.6	1.48	m	32.1	1.54	m
16	125.0	5.81	dd (3.4, 1.4)	22.1	2.02	m	23.6	1.93	m
16α				22.1	1.78	m	23.6	1.81	m
17	157.0			50.7	2.46	t (9.0)	52.1	2.41	t (9.4)
18	23.2	1.04	s	18.2	0.89	s	20.0	0.87	s
19	24.1	1.00	s	24.6	1.07	s	26.5	1.08	s
20	77.7			78.0	–		80.3	–	
21	22.6	1.31	s	21.0	1.17	s	22.7	1.19	s
22	77.1	3.59	m	78.6	3.32	m	80.2	3.39	m
23	26.4	1.45	m	27.5	1.29	m	29.0	1.31	m
23	26.4	1.66	m	27.5	1.68	m	29.0	1.64	m
24	41.9	1.45	m	42.6	1.81	m	43.7	1.48	m
24	41.9	1.81	m	42.6	1.44	m	43.7	1.77	m
25	71.2			71.5	–		74.0	–	
26	28.9	1.18	s	29.9	1.20	s	30.9	1.22	s
27	29.4	1.19	s	29.1	1.19	s	31.2	1.23	s

nd: not determined.

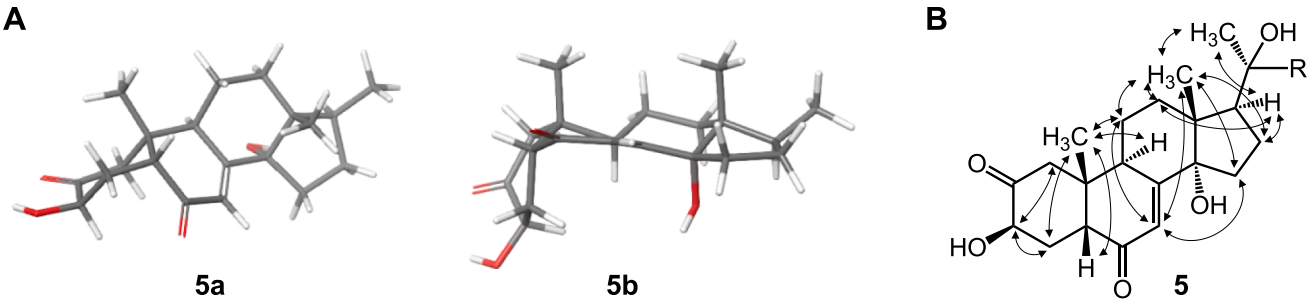

Fig. 2. The two major conformers of a model ring-system of compound **5**, **5a** and **5b** (**A**), and key NOE correlations observed in the ROESY spectrum of **5** (**B**).

calculated for the optimized geometries (Tables S13-14) as well. In comparison with the experimental values determined for **5**, the chemical shifts calculated for **5a** were in better agreement than those of **5b**. Beside these, the observed displacements in the chemical shift values of the A-ring protons and carbons compared to those of **6** (Table S17, Fig. S52) could also be better predicted by the calculated values of **5a** than with those derived for **5b** (Table S13, Fig. S51). Following the method and applying the templates provided by Grimblat, Zanardi and Sarotti [31], DP4 statistical parameters, introduced by Smith and Goodman [49], were also calculated for the two conformers. According to this analysis (Table S14), **5a** was predicted with 100% overall probability as the correct isomer.

Regarding the ROESY data, the spatial proximity of H-19/H-1βH-19/H-4β, H-19/H-5, H-19/H-11β, H-3/H-1α, H-3/H-4 α and H-5/ H-4β and that of H-19/H-11α could be explained with the **5a** conformation (Fig. 2). Further, the missing NOE correlation between H-3 and H-9 was also in agreement with the 5.1 Å distance of these protons in **5a**. Based on these results, **5** was characterized as a new ecdysteroid, i.e. the 2-dehydro-3β-hydroxyl derivative of 20E (**1**).

Based on the HRESIMS data, an elemental composition of $C_{54}H_{86}O_{13}$ was established for compound **11** (Fig. S34), nominally corresponding to a component formed by dimerization of **1** followed by dehydration of the resultant dimer.

Analysis of the methyl region of the ^{1}H and ^{13}C NMR spectra (Fig. S31) showed that **11** was a hetero-dimer, ie. two different monomeric units were connected. In comparision with the ^{1}H and ^{13}C NMR assignments of **1**, a closer inspection of the ^{13}C NMR data suggested that neither the A-ring nor the sidechain of the monomers were involved in the dimerization process. In addition, only one olefinic proton was detected in ^{1}H NMR spectrum of **11**, suggesting that in one of the

monomeric unit (m') C-7 was involved in the dimerization. In paralell, the presence of the characteristic resonances at 206.1, 169.9, 123.0 and 84.9 ppm in the ^{13}C NMR spectrum showed that in the other unit (m) the 6-keto-$\Delta^{7,8}$-14-OH moiety was still present. The common HMBC correlations of H-18 (0.73 ppm) and H-7 (5.83 ppm) with C-14 (84.9) and of H-19 (1.10) and H-7 with C-5 (53.5) and with C-9 (37.0) (Fig. S32) confirmed this suggestion and enabled the assigments of C-1, C-5, C-6, C-7, C-8, C-9, C-12, C-14 and C-17. HSQC correlations of these carbons (Fig. S33) led to the assignemnets of H-1, H-5, H-9, H-12 and H-17. Beside the correlation with H-7, H-9 (4.31 ppm) showed TOCSY correlation with a methine (from HSQC) at 2.34 ppm (H-11), suggesting that the dimerization took place via a C-11/C-7′ bond formation. In accordance with this, besides the correlations with C-1, C-5, C-7, C-11, C-12 and C-19, H-9 showed HMBC correlations with with C-7′ as well. The HMBC correlations of H-7′ (3.45 ppm) (from HSQC and TOCSY correlation with H-11) with C-6′, C-8′, C-9′, C-14′, C-11 and C-12 unamibigiously proved the C-11-C-7′ junction and suggested that in m' the hydroxyl group at C-14 was eliminated and a double bond formation between C-8 and C-14 took place. Based on these results the constitution shown in Fig. 1 was suggested for **11** that is a new ecdysteroid. Further analysis of the TOCSY, HSQC and HMBC confirmed this proposition and led to the complete ^{1}H and ^{13}C NMR assignment of **11** listed in Table 3.

Regarding the stereochemistry, based on the observed NOE correlations (Fig. S34,) between H-7′ (3.46 ppm) and H-5′ (2.50 ppm), H-19′ (0.91 ppm), H-15β (2.71 ppm), H-11 (2.34 ppm), H-1β (2.10 ppm) and H-19 (1.10), together with the correlations of H-11 (2.34 ppm) with H-18 (0.73 ppm) and with H-19 (1.10 ppm) confirmed that both H-7′ and H-11 are in beta position, thus the configuration of two new chiral centers C-7′ and C-11 are *S* and *R*, respectively.

In the case of **12**, HRMS data suggested an elemental composition of $C_{27}H_{42}O_7$ (Fig. S40). Thus, nominally, the incorporation of a double bond to the skeleton of **1**. Comparision of the ^{1}H and ^{13}C NMR spectra of **12** (Fig. S36) to those of **1** suggested that the oxidation did not affect the sidechain or the A- and B-rings. In the ^{1}H NMR spectrum, instead of the characteristic 3H intensity singlet of the angular methyl, H-18 (~0.9 ppm), two 1H intensity singlets were detected at 4.87 and 5.09 ppm. According to the HSQC data (Fig. S38), these alkenyl protons belong to the same carbon at 109.5 ppm. This suggested the presence of an endocyclic double bond in **12**. In the HMBC spectrum (Fig. S37), beside the correlation with C-17 (HMBC correlations with H-21 and H-22), the two alkenyl protons (H-18) showed correlations with a quternary carbon at 146.7 ppm (C-13) and to another methine (from HSQC) at 57.0 ppm (C-12). Based on these findings, cleavage of the C-13/C-14 bond and a double bond formation between C-13 and C-18 was envisaged.

Table 3
NMR assignments of compounds **10**, **12** and **13** in CD_3OD.

	m unit of 11				**m' unit of 11**			**12**			**13**		
Atom#	δ^{13}C, ppm	δ^{1}H, ppm	mult. (J in Hz)		δ^{13}C, ppm	δ^{1}H, ppm	mult. (J in Hz)	δ^{13}C, ppm	δ^{1}H, ppm	mult. (J in Hz)	δ^{13}C, ppm	δ^{1}H, ppm	mult. (J in Hz)
1β	40.5	2.10	m	1′	38.2	1.64	m	38.8	1.62	m	37.3	1.45	m
1α	40.5	1.55	m								37.3	1.80	m
2	68.3	4.42	m	2′	69.3	3.71	dt (11.8, 3.8)	69.0	3.86	ddd (11.4, 5.2, 2.9)	68.6	3.80	m
3	68.9	4.02	q (2.7)	3′	69.6	4.02	m	69.1	3.98	m	68.7	3.96	m
4β	32.9	1.93	m	4′	32.0	2.24	m	32.5	1.76	m	33.0	1.74	m
4α	32.9	1.69	m	4′	32.0	1.86		32.5	1.81	m			
5	53.5	2.35	m	5′	54.6	2.50	m	51.2	2.37	m	50.1	2.51	dd (12.47, 5.32)
6	206.1			6′	220.4			206.7			199.2		
7	123	5.83	d (2.7)	7′	55.9	3.46	d (2.5)	120.0	5.88	d (2.9)	144.9		
8	170			8′	129.5			175.9			125.0		
9	37	4.31	dd (8.2, 2.6)	9′	41.9	2.62	m	44.9	3.17	ddd (10.5, 7.1, 2.9)	38.3	2.77	dd (11.9, 5.9)
10	43.1			10′	39.0			40.9			40.0		
11β	40.3	2.34	m	11′	21.8	1.78	m	24.6	1.81	m	21.9	1.78	m
11α				11′	21.8	1.69	m	24.6	1.71	m			
12β	39.6	2.07	m	12′	39.4	2.24	m				41.0	2.29	m
12α				12′	39.4	1.34	m	57.0	2.35	m	41.0	1.56	br d (12.8)
13	47.6			13′	46.1			146.7			49.4		
14	84.9			14′	147.9			79.6			145.7		
15β	32.7	1.98	m	15′	27.4	2.37	dd (15.9, 1.4)	34.7	2.14	dt (12.5, 3.2)	134.0	6.47	t (2.9)
15α	32.7	1.56	m	15′	27.4	2.70	dd (15.9, 3.4)	34.7	1.62	m			
16	21.8	1.90	m	16′	22.2	2.09	dd (3.4, 1.4)	25.3	1.85	m	32.5	2.73	ddd (17.2, 11.0, 1.5)
16α	21.8	1.74	m	16′	22.2	1.64	m	25.3	2.07	m	32.5	2.22	ddd (17.2, 7.8, 3.7)
17	51.7	2.43	t (9.4)	17′	57.8	1.54	m	51.4	2.48	dd (13.0, 2.5)	57.7	2.06	dd (11.0, 7.7)
18	18.3	0.73	s	18′	19.7	1.21	s	109.5	5.09	s	20.7	1.13	s
								109.5	4.87	s			
19	24.7	1.10	s	19′	26.2	0.91	s	23.6	0.93	s	24.1	0.98	s
20	77.9			20′	77.8			77.1			77.4		
21	21.6	1.15	m	21′	21.1	1.25	s	19.6	1.29	s	20.6	1.25	s
22	78.5	3.25	dd (10.4, 1.3)	22′	78.3	3.40	m	76.3	3.88	m	78.7	3.37	dd (10.6, 1.7)
23	27.4	1.65	m	23′	27.7	1.52	m	26.6	1.69	m	27.4	1.62	m
23	27.4	1.31	m	23′	27.7	1.30	m	26.6	1.49	m	27.4	1.32	m
24	42.5	1.44	m	24′	42.4	1.39	m	42.0	1.46	m	42.4	1.43	m
24	42.5	1.81	m	24′	42.4	1.80	m	42.0	1.80	m	42.4	1.81	m
25	71.4			25′	71.4			71.6			71.4		
26	29.4	1.14	s	26′	29.6	1.14	s	29.1	1.20	s	30.0	1.20	s
27	29.4	1.20	s	27′	29.8	1.21	s	29.9	1.21	s	29.0	1.18	s

Furthermore, the HMBC correlation observed between H-7 and C-14 suggested a bond formation between C-12 and C-14 as well. The observed HMBC correlations (Fig. S37) of H-12 (2.35 ppm) with C-9 (44.9), C-14 (79.6) and C-13 (146.7 ppm) confirmed this structural proposition. Further analysis of the HSQC and HMBC data enabled the complete ^{1}H and ^{13}C NMR assignments of **12** (Table 3). Regarding stereochemistry, the similar spectral features observed for **12** and reported for **1** [45] suggested that the rearrangment did not affect the configuration of the C-2, C-3, C-5, C-9. C-10, C-17, C-20 and C-22 chiral centers. The NOE correlations detected in the ROESY spectrum of **12** (Fig. S39) were in accordance with this proposition. In addition, the spatial proximity of H-12 and H-9, H-17 and H_{α}-16 based on the observed NOE correlations between these protons together with those detected between H-17 and H_{α}-16, and between H-7 and $H_{\alpha,\beta}$-16 led to the conclusion that the ring opening and closing occured via a *trans* C/D ring fusion where H-12 occupied the α (12*S*) and the OH attached to C-14 occupied the β position (14*R*). Taking all these together, the structure shown in Fig. 1 was suggested for **12** that is a new ecdysteroid.

For compound **13**, a molecular formula of $C_{27}H_{42}O_7$ was established from the HRMS data (Fig. S45), again suggesting a double bond incorporation to the ring system of the parent compound **1**. As compared to the ^{1}H NMR data of **1**, the most striking difference in the case of **13** was the absence of the doublet signal characteristic for H-7 and the appearance of a triplet with 1H intensity at 6.47 ppm. Besides a somewhat upfielded (as compared to that in **1**) C-6 signal at 199.2 ppm, in the aromatic region of the ^{13}C NMR spectrum of **13** the signals of three quaternary carbons (145.7, 144.9, 125.0 ppm) and an sp^2 methine (134.0 ppm) were detected. The quaternary carbon at 145.7 was assigned to C-14 based on the HMBC correlation (Fig. S42) of this carbon with H-18 (1.10 ppm) (besides the usual correlations shown with C-12, C-13 and C-17). The resonances at 144.9 and 125.0 ppm were assigned to C-7 and C-8, respectively on the basis of the common HMBC correlations of H-5 (2.50 ppm) and H-9 (2.77 ppm) with C-7 and that of H-9 with C-8. The H-5 and H-9 signals were assigned by the HSQC correlations (Fig. S43) of C-5 and C-9, which latter were assigned based on the HMBC correlations of H-19 to them. Based on these findings, a double bond formation between C-14 and C-15, and the hydroxylation of C-7 was suggested in compound **13** (Fig. 1). Further analysis of the HSQC and HMBC data confirmed this structural proposition and enabled the complete ^{1}H and ^{13}C NMR assignments of **13** (Table 3). The characteristic NOE correlations (H-19/H-5, H-2/H-9, H-18/H-12β, H-16β) observed in the ROESY spectrum of **13** (Fig. S44) suggested that no inversion occurred during the oxidative formation of the compound. Taking all these together, the structure shown in Fig. 1 was proposed for **13** that is a new ecdysteroid.

3.4. Bioactivity on the Akt and AMPK phosphorylation

Compounds **2**–**4**, **7**, **9**, **12** and **15**, that were available in sufficient amounts, were tested for their capacity to interfere with the activation of protein kinase B (Akt) and AMP-activated protein kinase (AMPK). The tested compounds, **2**–**4**, **7**, **9**, **12** and **15** were 98.1, 98.7, 99.8, 97.2, 98.8, 99.8 and 99.2% pure, respectively, by means of HPLC-DAD, maximum absorbance within the range of 220–400 nm. Results are shown in Fig. 3.

The tested compounds were similarly active on the Akt phosphorylation as their parent compound 20E, and even though this was not statistically significant for compounds **4** and **7**, the tendency for these two was very similar to that of the others. Concerning the AMPK activation, however, stachysterone B (**7**) and a new ring-rearranged derivative (**12**) were the only significantly active derivatives. 20E, that was previously found to activate AMPKα via pAMPKα Thr^{172} [50], was inactive in our experimental setup. While the limited number of compounds tested in this study allowed only a modest evaluation of structure–activity relationships, compound **7** could still be compared with two derivatives that differ from it in only one moiety. These are 20E (retained 14α-OH) and compound **4** ($\Delta^{8,9}$ olefin instead of the $\Delta^{7,8}$). Accordingly, it may be concluded that a 14-OH elimination from 20E increases the AMPK activating activity, and that a retained $\Delta^{7,8}$ olefin is preferable in this regard.

The activation of Akt is a key effector of ecdysteroid action in mammals [14]. According to the recently proposed canonical mechanism of membrane action of ecdysteroids, the various bioactivities of these compounds may be explained via their activating effect on the Mas receptor, i.e. the G-protein-coupled receptor of angiotensin-(1–7) [51]. This would then lead to a rapid, Ca^{2+}-dependent activation of Akt

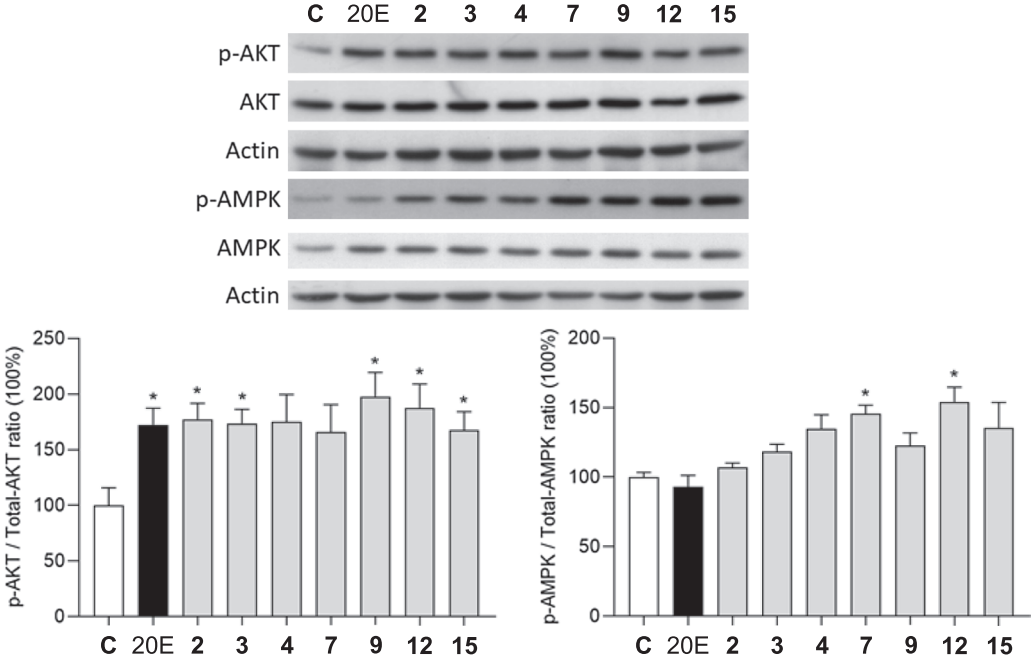

Fig. 3. The activity of compounds **2**–**4**, **7**, **9**, **12** and **15** on the phosphorylation of Akt and AMPK. *: $p < 0.05$ by means of one-way ANOVA followed by Dunnett's Multiple Comparisons test. Results are shown as mean ± SEM (n = 4).

[14,51], which kinase is therefore a rational choice to evaluate the potential of ecdysteroids for stimulating skeletal muscle protein synthesis [52], and for exerting their protective action on various tissues. Akt activation may also offer a potential strategy to ameliorate insulin resistance [53]. Accordingly, this mechanism has possible clinical relevance to the ongoing studies on 20-hydroxyecdysone for the treatment of sarcopenia [7] and prediabetes [8].

Further, the simultaneous activation of Akt and AMPK was recently suggested as the mechanism of action for improving the hepatic and possibly muscle glucose homeostasis in high-fat-high-fructose diet-fed rats [50]. The recently reported neuroprotective role of the Akt-AMPK interplay [54] may also be of interest concerning the *in vivo* neuroprotective action of ecdysteroids [26]. Nevertheless, further *in vitro* and *in vivo* studies need to be conducted for these compounds to verify their bioactivities and possible clinical applications.

4. Conclusions

To the best of our knowledge, this is the first report on the use of gamma radiolysis as a possible tool to expand the chemical diversity of ecdysteroids. The gamma irradiations of aqueous solutions of 20-hydroxyecdysone in N_2- or N_2O-saturated solutions resulted in the isolation of fourteen compounds of which five are new. Irradiations in N_2- or N_2O-saturated solutions resulted in complex mixtures presenting somewhat similar fingerprints but with different main products formed. A two-step isolation strategy was employed, including an initial fractionation by CPC with an uncommon *tert*-butyl alcohol containing biphasic solvent system, and subsequent preparative HPLC purification.

Our results on the compounds' activity on the Akt and, in two cases, the AMPK phosphorylation of skeletal muscle myotubes suggest their anabolic and cytoprotective effect, and particularly compounds **7** and **12** may act stronger in this regard than their parent compound 20E. These compounds are worthy for further investigation concerning their potential benefit against cardiovascular, metabolic, and/or central-nervous system pathologies.

Despite the relatively low yields of compounds obtained in this study, a great increase in chemical diversity and complexity was achieved, and this allowed the identification of valuable new bioactive compounds with unique chemical structures.

Declaration of Competing Interest

The authors declare that they have no known competing financial interests or personal relationships that could have appeared to influence the work reported in this paper.

Acknowledgments

This work was supported by the National Research, Development and Innovation Office, Hungary (NKFIH; K-134704), the Economic Development and Innovation Operative Program GINOP-2.3.2-15-2016-00012, and the Ministry of Human Capacities, Hungary grant 20391-3/2018/FEKUSTRAT.

Appendix A. Supplementary material

Supplementary data to this article can be found online at https://doi.org/10.1016/j.bioorg.2021.104951.

References

[1] L. Dinan, The Karlson Lecture. Phytoecdysteroids: what use are they? Arch. Insect Biochem. Physiol. 72 (3) (2009) 126–141.
[2] M. Báthori, N. Tóth, A. Hunyadi, A. Márki, E. Zádor, Phytoecdysteroids and anabolic-androgenic steroids–structure and effects on humans, Curr. Med. Chem. 15 (1) (2008) 75–91.
[3] A. Hunyadi, I. Herke, K. Lengyel, M. Báthori, Z. Kele, A. Simon, G. Tóth, K. Szendrei, Ecdysteroid-containing food supplements from Cyanotis arachnoidea on the European market: evidence for spinach product counterfeiting, Sci. Rep. 6 (2016) 37322.
[4] E. Isenmann, G. Ambrosio, J.F. Joseph, M. Mazzarino, X. de la Torre, P. Zimmer, R. Kazlauskas, C. Goebel, F. Botrè, P. Diel, M.K. Parr, Ecdysteroids as non-conventional anabolic agent: performance enhancement by ecdysterone supplementation in humans, Arch. Toxicol. 93 (7) (2019) 1807–1816.
[5] M.K. Parr, G. Ambrosio, B. Wuest, M. Mazzarino, X. de la Torre, F. Sibilia, J. F. Joseph, P. Diel, F. Botrè, Targeting the administration of ecdysterone in doping control samples, Forensic Toxicol. 38 (1) (2020) 172–184.
[6] https://www.wada-ama.org/sites/default/files/wada_2020_english_monitoring_program_.pdf. (Accessed 19.01.2020.
[7] https://clinicaltrials.gov/ct2/show/NCT03452488. (Accessed 19.11.2020.
[8] https://clinicaltrials.gov/ct2/show/NCT03906201. (Accessed 19.11.2020.
[9] A. Martins, N. Tóth, A. Ványolós, Z. Béni, I. Zupkó, J. Molnár, M. Báthori, A. Hunyadi, Significant Activity of Ecdysteroids on the Resistance to Doxorubicin in Mammalian Cancer Cells Expressing the Human ABCB1 Transporter, J. Med. Chem. 55 (11) (2012) 5034–5043.
[10] A. Hunyadi, J. Csábi, A. Martins, J. Molnár, A. Balázs, G. Tóth, Backstabbing P-gp: side-chain cleaved ecdysteroid 2, 3-dioxolanes hyper-sensitize MDR cancer cells to doxorubicin without efflux inhibition, Molecules 22 (2) (2017) 199.
[11] H.M. Issaadi, J. Csábi, T.J. Hsieh, T. Gáti, G. Tóth, A. Hunyadi, Side-chain cleaved phytoecdysteroid metabolites as activators of protein kinase B, Bioorg. Chem. 82 (2019) 405–413.
[12] R.G. Savchenko, M. Nové, G. Spengler, A. Hunyadi, L.V. Parfenova, In Vitro Adjuvant Antitumor Activity of Various Classes of Semi-synthetic Poststerone Derivatives, Bioorg. Chem. 104485 (2020).
[13] J. Csábi, T.J. Hsieh, F. Hasanpour, A. Martins, Z. Kele, T. Gáti, A. Simon, G. Tóth, A. Hunyadi, Oxidized Metabolites of 20-Hydroxyecdysone and Their Activity on Skeletal Muscle Cells: Preparation of a Pair of Desmotropes with Opposite Bioactivities, J. Nat. Prod. 78 (10) (2015) 2339–2345.
[14] J. Gorelick-Feldman, W. Cohick, I. Raskin, Ecdysteroids elicit a rapid Ca2+ flux leading to Akt activation and increased protein synthesis in skeletal muscle cells, Steroids 75 (10) (2010) 632–637.
[15] L. Wojnárovits, Radiation Chemistry, in: A. Vértes, S. Nagy, Z. Klencsár, R.G. Lovas, F. Rösch (Eds.), Handbook of Nuclear Chemistry, Springer, US, Boston, MA, 2011, pp. 1263–1331.
[16] Y. Blanco, G. de Diego-Castilla, D. Viúdez-Moreiras, E. Cavalcante-Silva, J. A. Rodríguez-Manfredi, A.F. Davila, C.P. McKay, V. Parro, Effects of Gamma and Electron Radiation on the Structural Integrity of Organic Molecules and Macromolecular Biomarkers Measured by Microarray Immunoassays and Their Astrobiological Implications, Astrobiology 18 (12) (2018) 1497–1516.
[17] G.G. Flores-Rojas, F. López-Saucedo, E. Bucio, Gamma-irradiation applied in the synthesis of metallic and organic nanoparticles: A short review, Radiat. Phys. Chem. 169 (2020), 107962.
[18] L.L. Smith, J.I. Teng, M.J. Kulig, F.L. Hill, Sterol metabolism. XXIII. Cholesterol oxidation by radiation-induced processes, J. Organic Chem. 38 (9) (1973) 1763–1765.
[19] M.P. Kane, K. Tsuji, Radiolytic degradation scheme for 60Co-irradiated corticosteroids, J. Pharm. Sci. 72 (1) (1983) 30–35.
[20] H. Fazakerley, Gamma irradiation of some unsaturated steroids, Int. J. Appl. Radiation Isotopes 9 (1) (1960) 130–132.
[21] J.A. LaVerne, OH radicals and oxidizing products in the gamma radiolysis of water, Radiat. Res. 153 (2) (2000) 196–200.
[22] A. Hunyadi, The mechanism (s) of action of antioxidants: From scavenging reactive oxygen/nitrogen species to redox signaling and the generation of bioactive secondary metabolites, Med. Res. Rev. 39 (6) (2019) 2505–2533.
[23] L. Fási, F. Di Meo, C.-Y. Kuo, S. Stojkovic Buric, A. Martins, N. Kúsz, Z. Béni, M. Dékány, G.T. Balogh, M. Pesic, H.-C. Wang, P. Trouillas, A. Hunyadi, Antioxidant-Inspired Drug Discovery: Antitumor Metabolite Is Formed in Situ from a Hydroxycinnamic Acid Derivative upon Free-Radical Scavenging, J. Med. Chem. 62 (3) (2019) 1657–1668.
[24] L. Fási, A.D. Latif, I. Zupkó, S. Lévai, M. Dékány, Z. Béni, Á. Könczöl, G.T. Balogh, A. Hunyadi, AAPH or Peroxynitrite-Induced Biorelevant Oxidation of Methyl Caffeate Yields a Potent Antitumor Metabolite, Biomolecules 10 (11) (2020) 1537.
[25] J.-Q. Dai, Y.-J. Cai, Y.-P. Shi, Y.-H. Zhang, Z.-L. Liu, L. Yang, Y. Li, Antioxidant Activity of Ecdysteroids from Serratula strangulata, Chin. J. Chem . 20 (5) (2002) 497–501.
[26] J. Hu, C.X. Luo, W.H. Chu, Y.A. Shan, Z.-M. Qian, G. Zhu, Y.B. Yu, H. Feng, 20-Hydroxyecdysone protects against oxidative stress-induced neuronal injury by scavenging free radicals and modulating NF-κB and JNK pathways, PLoS One 7(12) (2012) e50764-e50764.
[27] H.M. Issaadi, Y.C. Tsai, F.R. Chang, A. Hunyadi, Centrifugal partition chromatography in the isolation of minor ecdysteroids from Cyanotis arachnoidea, J. Chromatogr. B, Anal. Technol. Biomed. Life Sci. 1054 (2017) 44–49.
[28] J.B. Friesen, J.B. McAlpine, S.-N. Chen, G.F. Pauli, Countercurrent Separation of Natural Products: An Update, J. Nat. Prod. 78 (7) (2015) 1765–1796.
[29] M. Bojczuk, D. Żyżelewicz, P. Hodurek, Centrifugal partition chromatography - A review of recent applications and some classic references, J. Sep. Sci. 40 (7) (2017) 1597–1609.
[30] A.D. Bochevarov, E. Harder, T.F. Hughes, J.R. Greenwood, D.A. Braden, D. M. Philipp, D. Rinaldo, M.D. Halls, J. Zhang, R.A. Friesner, Jaguar: A high-performance quantum chemistry software program with strengths in life and materials sciences, Int. J. Quantum Chem. 113 (18) (2013) 2110–2142.

[31] N. Grimblat, M.M. Zanardi, A.M. Sarotti, Beyond DP4: an Improved Probability for the Stereochemical Assignment of Isomeric Compounds using Quantum Chemical Calculations of NMR Shifts, J. Organic Chem. 80 (24) (2015) 12526–12534.
[32] J.B. Friesen, G.F. Pauli, Rational development of solvent system families in counter-current chromatography, J. Chromatogr. A 1151 (1–2) (2007) 51–59.
[33] K. Kovács, Á. Simon, G.T. Balogh, T. Tóth, L. Wojnárovits, High-energy ionizing radiation-induced degradation of amodiaquine in dilute aqueous solution: radical reactions and kinetics, Free Radic Res 54 (2–3) (2020) 185–194.
[34] L. Canonica, B. Danieli, G. Lesma, G. Palmisano, Unusual photochemical behaviour of the enone chromophore of the insect moulting hormone 20α-hydroxyecdysone, J. Chem. Soc., Chem. Commun. (19) (1985) 1321-1322.
[35] J. Harmatha, M. Budĕšínský, K. Vokáč, Photochemical transformation of 20-hydroxyecdysone: production of monomeric and dimeric ecdysteroid analogues, Steroids 67 (2) (2002) 127–135.
[36] J. Harmatha, M. Budesínský, K. Vokác, Photochemical transformation of 20-hydroxyecdysone: production of monomeric and dimeric ecdysteroid analogues, Steroids 67 (2) (2002) 127–135.
[37] M.N. Galbraith, D.H.S. Horn, E.J. Middleton, R.J. Hackey, The structure of podecdysone B, a new phytoecdysone, J. Chem. Soc. D: Chem. Commun. (8) (1969) 402-403.
[38] N. Nishimoto, Y. Shiobara, S.-S. Inoue, M. Fujino, T. Takemoto, C.L. Yeoh, F. de Oliveira, G. Akisue, M.K. Akisue, G. Hashimoto, Three ecdysteroid glycosides from Pfaffia iresinoides, Phytochemistry 27 (6) (1988) 1665–1668.
[39] A. Simon, G. Tóth, E. Liktor-Busa, Z. Kele, M. Takács, A. Gergely, M. Báthori, Three new steroids from the roots of Serratula wolffii, Steroids 72 (11–12) (2007) 751–755.
[40] W.-M. Zhu, H.-J. Zhu, W.-S. Tian, X.-J. Hao, C.U. Pittman, The selective dehydroxylation of 20-hydroxyecdysone by Zn powder and anhydrous acetic acid, Synth. Commun. 32 (9) (2002) 1385–1391.
[41] K. Vokac, M. Budesinsky, J. Harmatha, Minor Ecdysteroid Components of Leuzea carthamoides, Collect. Czech. Chem. Commun. 67 (2002) 124–139.
[42] A. Suksamrarn, S. Charoensuk, B.-E. Yingyongnarongkul, Synthesis and biological activity of 3-deoxyecdysteroid analogues, Tetrahedron 52 (32) (1996) 10673–10684.
[43] A. Hunyadi, A. Gergely, A. Simon, G. Tóth, G. Veress, M. Báthori, Preparative-scale chromatography of ecdysteroids of Serratula wolffii Andrae, J. Chromatogr. Sci. 45 (2) (2007) 76–86.
[44] M. Kiuchi, H. Yasui, S. Hayasaka, M. Kamimura, Entomogenous fungus Nomuraea rileyi inhibits host insect molting by C22-oxidizing inactivation of hemolymph ecdysteroids, Arch. Insect Biochem. Physiol. 52 (1) (2003) 35–44.
[45] M. Budĕšínský, K. Vokáč, J. Harmatha, J. Cvačka, Additional minor ecdysteroid components of Leuzea carthamoides, Steroids 73 (5) (2008) 502–514.
[46] R. Savchenko, S. Kostyleva, V. Odinokov, L. Parfenova, K. Kitaev, E. Surina, G. Benkovskaya, Protective effects of semi-synthetic ecdysteroids in the Colorado potato beetle adult under chronic and acute toxic stress, Евразиатский энтоМологический Журнал 16 (5) (2017) 446–449.
[47] S.D. Sarker, V. Šik, H.H. Rees, L. Dinan, 2-dehydro-3-epi-20-hydroxyecdysone from Froelichia florida, Phytochemistry 49 (8) (1998) 2311–2314.
[48] J.-P. Girault, C. Blais, P. Beydon, C. Rolando, R. Lafont, Synthesis and nuclear magnetic resonance study of 3-dehydroecdysteroids, Arch. Insect Biochem. Physiol. 10 (3) (1989) 199–213.
[49] S.G. Smith, J.M. Goodman, Assigning Stereochemistry to Single Diastereoisomers by GIAO NMR Calculation: The DP4 Probability, J. Am. Chem. Soc. 132 (37) (2010) 12946–12959.
[50] J. Buniam, N. Chukijrungroat, Y. Rattanavichit, J. Surapongchai, J. Weerachayaphorn, T. Bupha-Intr, V. Saengsirisuwan, 20-Hydroxyecdysone ameliorates metabolic and cardiovascular dysfunction in high-fat-high-fructose-fed ovariectomized rats, BMC Complementary Medicine and Therapies 20 (1) (2020) 140.
[51] R. Lafont, S. Raynal, M. Serova, B. Didry-Barca, L. Guibout, M. Latil, P.J. Dilda, W. Dioh, S. Veillet, 20-Hydroxyecdysone activates the protective arm of the renin angiotensin system via Mas receptor, bioRxiv (2020) 2020.04.08.032607.
[52] S. Schiaffino, C. Mammucari, Regulation of skeletal muscle growth by the IGF1-Akt/PKB pathway: insights from genetic models, Skeletal Muscle 1 (1) (2011) 4.
[53] Z. Zhang, H. Liu, J. Liu, Akt activation: A potential strategy to ameliorate insulin resistance, Diabetes Res Clin Pract 156 (2019), 107092.
[54] M. Jovanovic-Tucovic, L. Harhaji-Trajkovic, M. Dulovic, G. Tovilovic-Kovacevic, N. Zogovic, M. Jeremic, M. Mandic, V. Kostic, V. Trajkovic, I. Markovic, AMP-activated protein kinase inhibits MPP+-induced oxidative stress and apoptotic death of SH-SY5Y cells through sequential stimulation of Akt and autophagy, Eur. J. Pharmacol. 863 (2019), 172677.